Journal of Power Electronics (2021) 21:1878–1887
https://doi.org/10.1007/s43236-021-00321-w

ORIGINAL ARTICLE

LLC inverter design for driving surface DBD optimized for airborne bacteria inactivation

Yeong Woon Kim[1,2] · Thusita Randima Wellawatta[1,3] · Sung-Jin Choi[3] · Jun Choi[1]

Received: 29 April 2021 / Revised: 29 September 2021 / Accepted: 1 October 2021 / Published online: 27 October 2021

Abstract

This paper proposes a design for an LLC resonant inverter with reflecting plasma characteristics to improve indoor air quality. A surface dielectric barrier discharge (SDBD) helps improve indoor air quality since it effectively inactivates airborne bacteria. By collaborating with plasma physics and power electronics, this study electrically models the SDBD structure. Thus, it presents a compact and commercially viable plasma generation circuit to drive the SDBD feature. The traditional LLC inverter design procedure is not optimized for such an application due to utilization differences. An LLC resonant inverter operating in the resonant mode combined with a step-up transformer is optimally designed to generate a 4-$kV_{pk\text{-}pk}$, 7.8-kHz sinusoidal voltage with a total power consumption of less than 2.5 W. By investigating optical emission spectroscopy (OES), the production of a reactive species for the inactivation of airborne bacteria is confirmed. Furthermore, the sterilization performance is tested by observing the removal rate of the *Staphylococcus epidermidis* (*S. epidermidis*) bacteria inside a 1 m^3 chamber.

Keywords LLC inverter · Plasma generation · Surface dielectric barrier discharge · Sterilization · Airborne bacteria

1 Introduction

Due to the recent development of industry, air has become seriously polluted. There has been a significant increase in the amount of dust, fumes, bacteria, and harmful gases, resulting in problems such as various respiratory diseases and secondary infections due to sepsis, urinary tract infections, and endocarditis [1–3]. Therefore, social interest and demand for air purifiers that can sterilize airborne pathogenic microorganisms such as bacteria and viruses are growing. The plasma-based sterilization of airborne bacteria is one way to purify air [4]. Reactive species produced through plasma can be sterilized by destroying bacterial cell membranes or by suppressing DNA growth. This can sterilize airborne bacteria that are harmful to the human body [5, 6]. There are three challenges in the application of plasma drivers. The first challenge is to provide optimal plasma generation power to improve the sterilization performance of plasma generators. High-voltage and low-current drive specifications in AC or pulse power are required for atmospheric plasma generation [7, 8]. The second challenge requires a structural understanding of plasma generators and an analysis of plasma characteristics. A plasma generator is made with a surface dielectric barrier discharge (SDBD) for improving contact with bacteria. Thus, an appropriate model should be made [9]. The third and most critical challenge is commercialization. Conventionally, various techniques have been used to generate a sufficient plasma voltage even though most of the systems show acceptable performance. However, it is a challenge to implement such techniques as a commercial product.

Existing plasma generator studies can be classified as unipolar pulse, DC, and sinusoidal voltage systems. Most plasma-oriented researches use a high-voltage amplifier to obtain the required voltage at the laboratory level. Pulse voltages is used in some studies with a half-wave rectified fly-back converter for practical applications. The fly-back

✉ Jun Choi
junchoi@kitech.re.kr

1 Advanced Forming Process R&D Group, Korea Institute of Industrial Technology, Ulsan, Korea

2 School of Electronics and Electrical Engineering, College of IT Engineering, Kyungpook National University, Daegu, Korea

3 Department of Electrical, Electronic and Computer Engineering, University of Ulsan, Ulsan, Korea

transformer only utilizes the first quadrant of the B-H curve, which results in a bulky size.

In DC plasma systems, a Cockcroft–Walton voltage multiplier circuit is used in many kinds of research [10, 11]. It is suitable for micro-power ionizer applications. Thus, pulse and DC plasma systems are not suitable for domestic air purifiers. On the other hand, an AC plasma system can mitigate all the above disadvantages. A full-bridge converter with multiple resonant networks [12, 13] is proposed. However, it possesses circuit complexity, high cost, and implementation difficulties. In terms of the system, microwave plasma is also applicable to plasma generation. However, it is difficult to use for domestic appliances due to price and size limitations [14].

An LLC inverter provides cost-effectiveness for commercial air purifiers. In this paper, a half-bridge LLC is adopted. Since it is designed for an input voltage of DC 12 V, it can also be operated by batteries. It consists of a two-stage structure capable of DC–AC and AC–AC conversion. The first stage converts DC 12 V into a sinusoidal voltage with a fixed amplitude and frequency through an LLC network using a PWM controller [15]. In the second stage, the AC voltage is amplified by a step-up transformer with a high turns ratio to supply high voltage to the SDBD [16].

This study intends to develop a low-cost straightforward high-voltage generator for a domestic air purifier that improves the inactivation rate of airborne bacteria. For the experiment, *Staphylococcus epidermidis* (*S. epidermidis*) bacteria were used to test the inactivation rate [17].

2 Modeling of the SDBD

2.1 Principle of operation

The SDBD is made of two electrodes separated by a dielectric material, as shown in Fig. 1a. It is similar to the basic structure of a capacitor. However, the capacitance of the SDBD is proportional to the overlap area of the electrode, where higher capacitance decreases the output impedance so that the plasma voltage is decreased. Therefore, overlapping areas between the electrodes should be minimized to reduce the capacitance of the SDBD. When the electric field is enough to detach electrons from atoms in the air, plasma occurs in the air near the edge of the electrodes bounded to the opposite electrode area. Here, the electric field goes parallel to the dielectric layer near the edge of the electrodes and tends to the opposite side electrode through the dielectric layer, as shown in Fig. 1b.

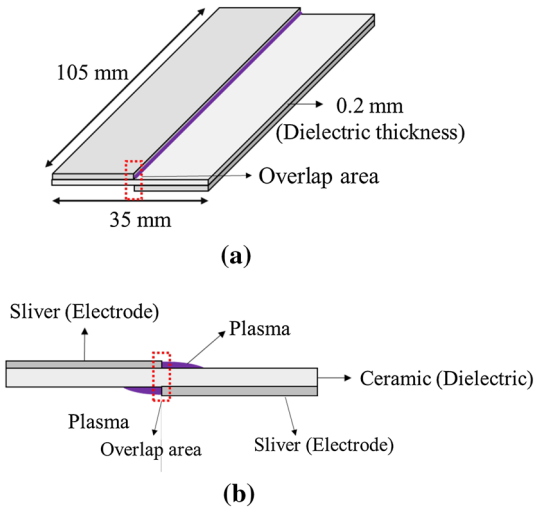

Fig. 1 Configuration of the SDBD: (**a**) 3D view; (**b**) side view

2.2 Electrical equivalent modeling of the SDBD

The electrical model of the SDBD has many definitions and arguments. A five capacitor model was proposed, where the parasitic capacitance of the electrodes is dominant, and the other capacitors inject harmonics to imitate the plasma current [9]. On the other hand, a series of capacitors and resister equivalent circuits was formed and presented in [18]. This model was verified for "n" number of the units. Another simple model was proposed in [19] in the no power case, the SDBD is equivalent to two series capacitors. When plasma is activated, one capacitor is changed into a parallel network of a capacitor and a resistor.

Ideally, The SDBD has an infinite resistance and zero capacitance between electrodes. However, its electrodes create a parasitic capacitance, and the dielectric has a significant resistance in practice. Thus, the equivalent circuit model can be identified as a parallel resistor, as shown in Fig. 2. Here, R_L describes the dissipation in the dielectric layer, and C_L characterizes the parasitic charge stored between the two electrodes. In this study, C_L is assumed to be constant, while the plasma operation and R_L are changed due to the plasma. This dynamic resistance is used to determine the properties of the LLC inverter.

2.3 Extraction of model parameters

The parasitic capacitance of the SDBD can be measured by an LCR meter. Typically, under the no power condition, C_L has a value from 10 to 1000 pF, and R_L of the SDBD is difficult to measure due to its extremely high value. When activating plasma, air atoms are ionized and detached into

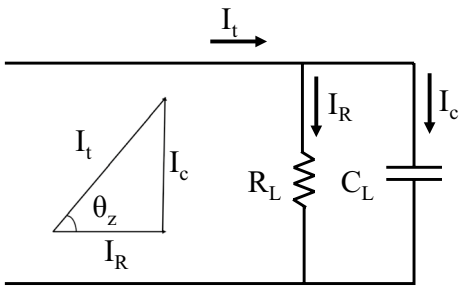

Fig. 2 Equivalent circuit of the SDBD (CL is made by area of the SDBD electrode edge and the thickness of the dielectric)

electrons and cations [11]. This process consumes a small spike current. When this ionization continuously occurs, the SDBD current becomes a spike burst that shows active power consumption. Such power consumption can be measured by using special power integration techniques such as Lissajous curves [20]. They can be used to calculate the equivalent dynamic resistance of the SDBD based on the phase angle. Thus, the load current and voltage of the SDBD show a pure capacitive behavior. In the peak and valley of the voltage waveform, a current spike burst is superimposed. By LCR meter measurements, $C_L = 10$ pF and $R_L{}^* = 100$ MΩ are obtained.

2.4 Circuit requirements for plasma generation

The factors of plasma generation are widely discussed in Paschen's law [20]. Under atmospheric pressure, the breakdown voltage of plasma generation can be calculated according to the dielectric thickness of the SDBD. For the target SDBD, the atmospheric pressure is 101.325 kPa, and the dielectric thickness is 0.2 mm. Thus, the pressure on the dielectric thickness (Pd) becomes 101.325 kPa × 0.02 cm, which is 2.0265 kpa·cm. According to Paschen's curve, the breakdown voltage related to the Pd is about 3.6 $kV_{pk\text{-}pk}$, which is the minimum voltage condition to initiate plasma generation.

Plasma behavior according to frequency change is discussed in [21], where it has been confirmed that a 1 kHz to 10 kHz operating frequency is usually recommended for SDBD applications.

3 Proposed plasma generator circuit

3.1 LLC inverter review

Generally, the voltage gain of an LLC resonant tank is kept at around unity. In addition, the zero voltage switching (ZVS) condition is available in that frequency region. Moreover, the load-independent converter gain and frequency-controlled close loop operations are available in this region. A detailed LLC transformer design process was presented in [22]. However, this study only requires a step-up sinusoidal inverter. Thus, the LLC topology is highly suitable. Due to its low input voltage, the switching-loss can be less critical. The resonant point can be used as the operating point to utilize the maximum voltage gain. Thus, a minimally distorted sinusoidal waveform can be generated. Moreover, the transformer gain is also used to achieve the target voltage. In addition, galvanic isolation of the transformer improves the safety of the inverter.

3.2 Circuit design procedure

The designed LLC resonant inverter in Fig. 3 consists of a half-bridge with two MOSFET switches, a capacitor (C_r), a leakage inductance (L_r), and the magnetizing inductance (L_m) of the transformer. The complementary gating signals produced by the gate driver are applied at the gates of the two MOSFETs. This generates a square wave voltage on the common node of the MOSFETs. The generated waveform excites the resonant tank and produces a sinusoidal voltage on the primary side of the transformer. To satisfy the minimum voltage requirement, a 4 $kV_{pk\text{-}pk}$ output voltage is used.

For economic capacitor voltage rating selection, the maximum resonant capacitor voltage is limited to 250 V. Thus, the maximum primary voltage at resonance can be calculated using the capacitor voltage equation ($V_r = V_l$ at resonance). In addition, the maximum peak voltage of the primary is decided as:

$$V_{pk,\max} = 250 \times 0.5 = 125\, V_{pk} = 250\, V_{pk-pk,\max} \tag{1}$$

In the transformer design process, the voltage step-up ratio is taken as 200 $V_{pk\text{-}pk}$ to 4 $kV_{pk\text{-}pk}$. Then, the transformer ratio n becomes:

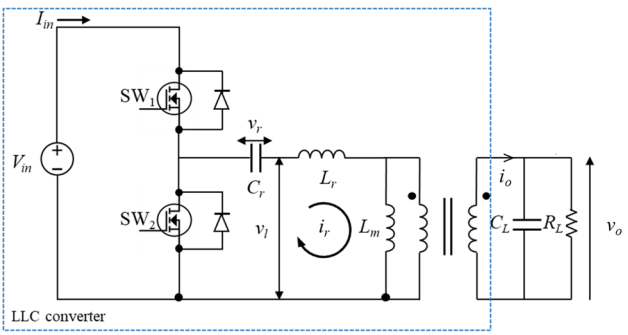

Fig. 3 Basic structure of a half-bridge converter with a resonant tank and a DBD load (CL and RL make up the SDBD equivalent circuit)

$$n = \frac{N_p}{N_s} = \frac{V_p}{V_o} = \frac{1}{2} \tag{2}$$

where V_p and V_o are the primary and secondary voltages, and N_p and N_s are the transformer primary and secondary turns, respectively. Then, the transformer input becomes:

$$V_p = nV_s = 200V_{pk-pk} = 100\ V_{pk.} \tag{3}$$

Due to the large turn ratio, the primary leakage inductance is assumed to be about 20%. Then:

$$V_l = V_p + V_p \bullet 20\ \% = 120\ V_{pk}. \tag{4}$$

When the input voltage is 12 V, the required minimum Q-factor (Q_0) for the target V_1 can be calculated as:

$$Q_{0,min} = \frac{V_1}{V_{in}} = 10. \tag{5}$$

For plasma operation, the target frequency range is taken as 5 kHz ~ 10 kHz, and 7.5 kHz is used to initialize the design process. Accordingly, the transformer design requirements are noted in Table 1, and the transformer design steps in [23] are followed.

Table 1 Transformer design parameters of the target system

Parameter		Value
V_{in}	Input voltage	84 V_{rms}
V_o	Output voltage	1414 V_{rms}
I_o	Output current	1.06 mA_{rms}
P_o	Output power	1.5 W
f	Frequency	7.5 kHz
η	Efficiency	0.95
A	Regulator	5%
B_{ac}	Operating flux density	0.3 teslas
K_u	Window utilization	0.4
T_r	Temperature rise goal	30 ℃
K_f	Waveform coefficient	4.44

Consequently, the required minimum core geometry (K_g) factor is calculated as 0.00029 cm^5. By considering different types of cores, ER2834 is selected due to a large enough window areas that satisfies other technical requirements with a smallest size. Then, the primary turns become 105 T. According to $A_{wp(B)}$, the primary wire size is selected 0.6 mm (23 AWG). Then, the secondary winding can be calculated. Due to the window limitation of the sector partition in the bobbin, N_p is limited to 100 T, and N_s is taken as 2000 T to maintain the turn ratio in (2). Then, the primary inductance of the transformer (L_p) becomes 4.1 mH, L_r becomes 0.765 mH, and R_p becomes 2.8 Ω. Thus, L_m can be calculated as 3.335 mH. In accordance with the required frequency range, the resonant capacitance can be calculated as (6).

$$f_r = \frac{1}{2\pi\sqrt{(L_p * C_r)}} \Rightarrow C_r = \frac{1}{(2\pi f)^2 * L_p} = 109\ nF \tag{6}$$

By adopting a 100 nF capacitor for the Cr, the resonant frequency becomes 7.8 kHz. The resonant frequency achieves its maximum voltage gain when the impedance becomes purely resistive and the maximum current flows [13, 24]. The selected parameters of the LLC inverter are shown in Table 2.

3.3 Transformer performance analysis

According to the transformer design, an equivalent circuit of a load with a transformer can be analyzed. The plasma load current and voltage are observed. Here, the phase angle (θ) is observed as 54°, and the dynamic resistance is obtained as shown in Table 3. Then, the reflected resistance in the

Table 3 Dynamic Electrical Properties of the SDBD

Parameter	Value
X_c	2 MΩ
I_c	1 mA
I_R	0.73 mA
R_L	2.74 MΩ

Table 2 Selected properties of an LLC resonant inverter with the SDBD

Parameter		Value	Parameter		Value
V_{in}	Input voltage (V)	12	C_r	Series capacitance (nF)	100
I_{in}	Input current (mA_{avg})	200	R_{cr}	ESR (Ω)	0.001
v_o	Load voltage (kV_{pk-pk})	4	L_p	Primary inductance (mH)	4.1
i_o	Load current (mA_{pk-pk})	16	L_r	Leakage inductance (μH)	765
v_r	Resonant voltage (V_{pk-pk})	220	L_m	Magnetizing inductance (mH)	3.335
R_p	Primary resistance (Ω)	2.8	C_L	Load capacitor (pF)	10
i_r	Resonant current (A_{pk-pk})	1.4	R_L^*	Without plasma resistance (MΩ)	100
f_r	Resonant frequency (kHz)	7.8	R_L	With plasma resistance (MΩ)	2.74

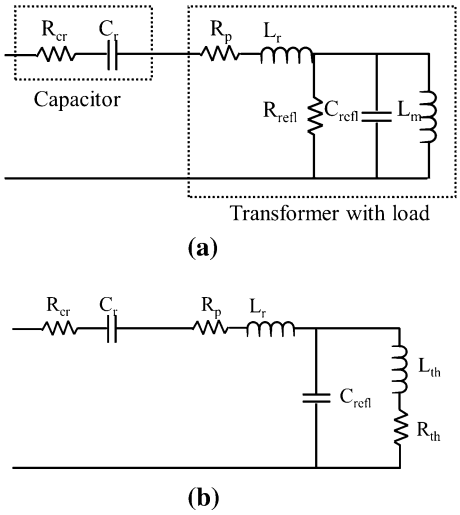

Fig. 4 Equivalent circuit of a transformer: (**a**) reflected primary impedance of the SDBD; (**b**) simplified thevenin impedance of the SDBD

primary of the transformer can be calculated by using (7) as shown in Fig. 4a.

$$Z_p = n^2 Z_s \rightarrow \frac{1}{Z_p} = \frac{1}{6880} + \frac{1}{5000j.} \tag{7}$$

Thus, R_{refl} and C_{refl} become 6.88 kΩ and 4 nF, respectively. Here, another resonant circuit that contains C_{refl} and L_m can be identified, and its resonant point can be calculated as 50 kHz by using (6). It is much further from the fundamental resonant frequency and can be identified as a ripple in the load current. In the case of R_{refl}, the Thevenin resistance can be used to calculate the dynamic Q-factor as shown in Fig. 4b.

$$Z_{th} = \frac{R_{refl} * X_{Lm}}{R_{refl} + X_{Lm}} = 3.88 + j163.35, \tag{8}$$

$$L_{th} = \frac{163.35}{2\pi f} = 3.33\ mH. \tag{9}$$

The load resistance is changed rapidly in the open circuit and dynamic resistance due to the plasma effect. Thus, two Q-factors exist in such a system as calculated in Table 4 by using (10).

$$Q_0 = \frac{1}{R_{cr} + R_p + R_{th}} \sqrt{\frac{L_p}{C_r}} \tag{10}$$

This causes a current burst in the peak and valley of the voltage wave. This Q-factor satisfies the minimum design requirements, and hardware is implemented accordingly.

Table 4 Changes in the Q-factor according to the dynamic resistance of the SDBD

Parameter	No plasma	With plasma
$1/Z_p$	1/250 k + 1/5000 j	1/6880 + 1/5000 j
Z_{th}	0.11 + j163.44	3.88 + j163.35
Q-factor	69.5	30.3

4 Verifications

4.1 Simulation verification

The designed system is implemented on PSIM for simulation, as shown in Fig. 5. Here, the gating signals are generated by C-block. In the resonant tank, 0.001 Ω is used for the equivalent series resistance (ESR) of the resonant capacitor. The transformer is simulated as an ideal transformer with leakage inductance and magnetizing inductance. Finally, the excitation waveform (V_x), transformer primary voltage (V_l), and output voltage (V_o) are plotted in Fig. 6. Here, 7.8 kHz is located at the peak of the voltage gain and it produces the target voltage. The plasma load is simulated on COMSOL. For the sterilization of airborne bacteria, plasma should be formed on the surface to facilitate contact with germs. Sterilization efficiency is also increased in the same space through plasma generation on both sides to expand the contact area with bacteria [7]. The designed electrodes are analyzed using COMSOL multiphysics. In the simulation, the electrodes and dielectric were fabricated with silver and ceramic, respectively. It was constructed as shown in Fig. 7. Here, 4 $kV_{pk\text{-}pk}$ 7.8 kHz is supplied to maintain the electric field up to 3.3×10^6 V/m. The SDBD is designed to obtain sufficient electric fields for plasma generation.

4.2 Hardware Implementation

The power inverters for air purifiers are designed for the lowest possible volume and power. Therefore, a minimum

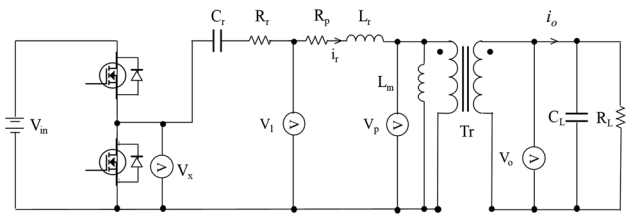

Fig. 5 PSIM simulation schematic diagram (Vx: excitation voltage, Vl: transformer primary voltage, Vo: output voltage, Io: output current, ir: resonant current)

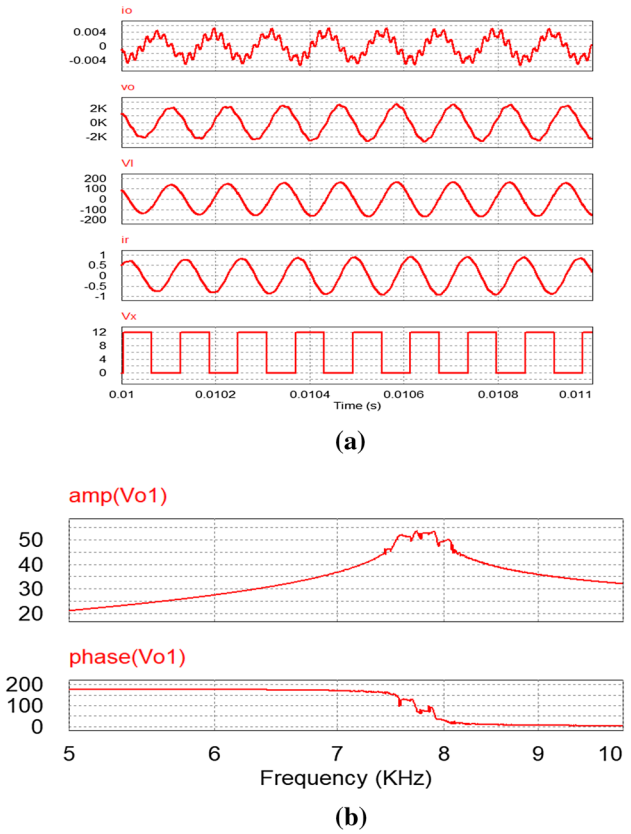

Fig. 6 Psim simulation results: (**a**) simulation waveforms; (**b**) frequency response of the LLC network

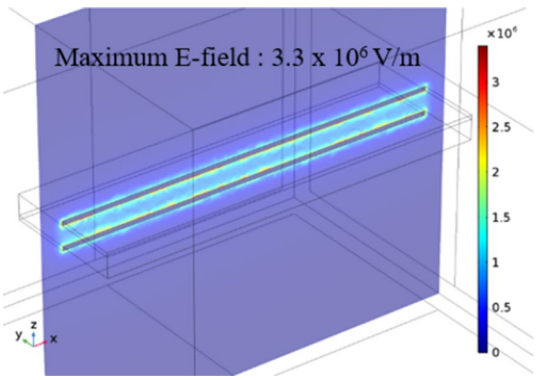

Fig. 7 Calculation of the electric field in the SDBD structure through COMSOL multiphysics

component count is essential, and the transformer, which occupies most of the volume in a power supply, should be optimally designed. For the final prototype, a 2.5 W power, 60(L) × 60(W) × 28(H) mm-sized inverter was designed.

An overall block diagram of the hardware circuit is shown in Fig. 8. In the gate signal stage, single 5 V logic signals are fed into the gate driver IC, which drives the MOSFET

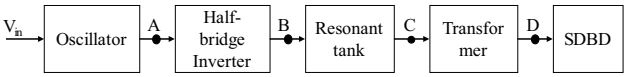

Fig. 8 Block diagram of an LLC resonant converter (**A**): input of the inverter, (**B**): excitation of the resonant tank, (**C**) primary of the transformer, (**D**): output of the LLC resonant converter)

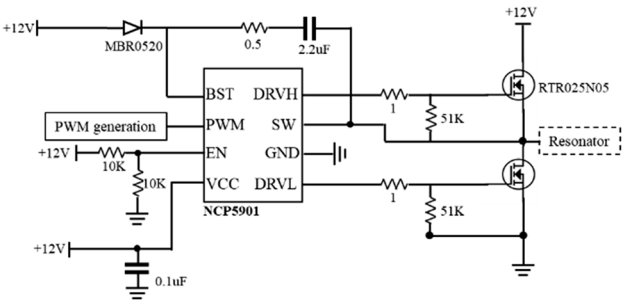

Fig. 9 Configuration of a gate driver: high side and low side MOSFET driving with a boost trap circuit

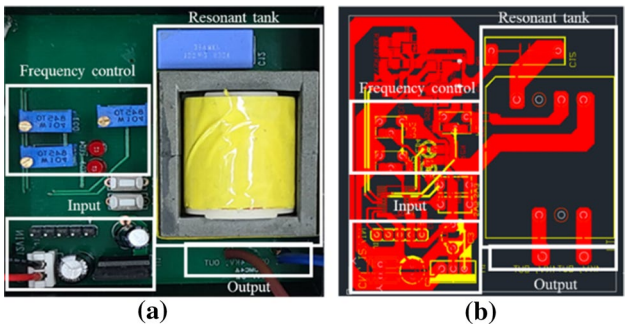

Fig. 10 LLC resonant converter (60 × 60 × 28 mm board): (**a**) hardware implementation; (**b**) PCB artwork

pair in a complementary manner, as shown in Fig. 9. Finally, the prototype of the LLC inverter is fabricated according to Fig. 10a, and its printed circuit board (PCB) design artwork is shown in Fig. 10b. To confirm the utilization of the inverter, an evaluation of the target sterilization performance is essential. Thus, an SDBD application setup is prepared. For the first time, a reduction experiment of airborne bacteria was conducted through an SDBD. Serial dilution, spray, sampling, and incubation processes must be carried out to obtain the reduction rate of *S. epidermidis*. The population of *S. epidermidis* sprayed into the air is set by performing series dilution. The supply of *S. epidermidis* was purchased from the Korea Collection for Type Cultures (KCTC). *S. epidermidis* was distributed in a 10 ml spot solution sterilized by a high-pressure steam sterilizer. An initial homogeneous mixture was produced using a vortex mixer (Talboys). The serial dilution method was used to dilute n

times by transferring 1 ml of the initial homogeneous mixture to 9 ml of distilled water. Next, 0.1 ml of the homogeneous mixture diluted to 10^{-n} was sprayed on 15 ml of solid medium (trypticase soy agar, TSA) and applied evenly to the solid medium using a spreader. The bacteria transferred to the solid medium were cultured 24 h at 37 °C by a culture medium (Bionex, VS-3DMC). The incubation results are obtained by counting the number of colony-forming units (CFUs) and calculate the initial condition by dividing 10^{n} of the diluted homogeneous mixture. In addition, airborne bacteria experiments were conducted by spraying *S. epidermidis* into a chamber of 1 m^3. The chamber consists of a 1 m^3 space, a nebulizer, two fans, and an air sampler. A 55 W UV lamp was installed in the chamber to sterilize the space before the experiment.

4 ml of the homogeneous mixture diluted to 10^{-2} was sprayed into the chamber with a nebulizer for 20 min, and the air before and after plasma treatment is sampled into the solid medium through a air sampler for 1 min.. After incubating for 24 h, the reduction rate is determined by comparing the number of CFUs. It is also necessary to analyze whether the SDBD produced reactive species valid for sterilization. When the plasma was generated, various reactive oxygen species (ROS) and reactive nitrogen species (RNS) were produced, such as O, N_2, and NO. The generated reactive species can sterilize germs by oxidizing the cell membranes or by sterilizing the bacteria by oxidizing the cell membrane or DNA. In addition, the authors of [28] demonstrated a process for producing a second positive system of the nitrogen spectrum and an reactive species valid for sterilization through the atomic oxygen spectrum.

To analyze the properties of the plasma, an optical emission spectroscopy (OES) can be used to analyze the plasma spectrum, which can be monitored by converting particle illuminant into spectra from specific wavelengths [4, 29, 30].

4.3 Hardware verification

Hardware waveforms are shown in Fig. 11. In the implementation of hardware, a linear regulator (LM7805) is used to power up the PWM generator [25, 26]. The PWM signals in Fig. 11a show that the half-bridge converter produces a pulse waveform as shown in Fig. 11b, which is further changed to a sinusoidal voltage by the LLC resonant network. The voltage is increased at the resonant frequency due to the high Q-factor, which results in a voltage waveform like that shown in Fig. 11c. Next, the ratio step-up transformer amplifies the voltage, which results in the waveforms shown in Fig. 11d.

Unlike the simulation of the transformer model, the real transformer has different core losses and skin effects. In the output current, the plasma makes a spike current, which is not available in the simulation. However, it does not have a considerable impact on the final performance due to the low switching frequency and the fact that the current spikes have a comparatively low energy level when compared with the stored energy in the resonant tank. It is demonstrated that the prototype can deliver enough voltage and enough of target frequency to generate plasma. The performances of

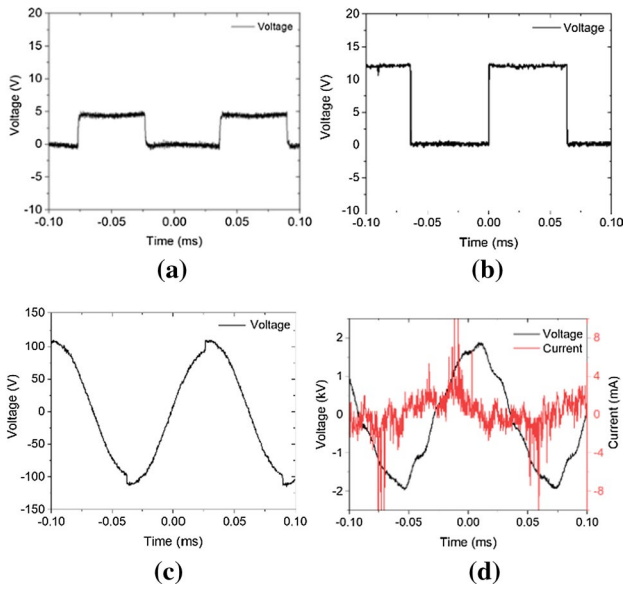

Fig. 11 Testing waveforms of an LLC resonant converter: (**a**) PWM for the gate driver; (**b**) complementary node signal; (**c**) waveform of the transformer primary; (**d**) DBD waveform

Table 5 Comparison of electrical properties

Parameter	Simulation	Hardware
V_l	200 $V_{pk\text{-}pk}$	220 $V_{pk\text{-}pk}$
V_o	4 $kV_{pk\text{-}pk}$	4 $kV_{pk\text{-}pk}$
f	7.8 kHz	7.86 kHz

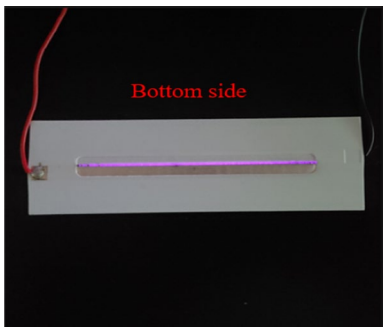

Fig. 12 SDBD with plasma generated by applying a power supply, with 4 kVpk-pk, 7.8 kHz

the hardware and simulation studies nearly coincided with each other. A comparison of the result is shown in Table 5.

By using the prototype system, air purification performance is observed. The SDBD is fabricated and powered up using the designed LLC inverter, as shown in Fig. 12. During operation, the result of OES was observed, as shown in Fig. 13. The emission intensity generated through the OES is expressed relatively at the time set by an arbitrary unit. When the OES results of the bottom surface of the plasma generation area were analyzed, it was shown to consist of a second positive system of nitrogen and the atomic oxygen spectrum at atmospheric pressure. The second positive system of the nitrogen spectrum is dominant, with the highest intensity occurring at a wavelength of 337 nm. In addition, atomic oxygen typically occurs at a wavelength of 380 nm. However, its results are mainly at wavelengths of 493.16 nm. The OES results of the manufactured sterilization module support its ability to inactivate airborne bacteria [29]. The complex chemical formula in the generation of ROS and RNS by atmospheric pressure plasma were demonstrated by [6] and [30]. When the two demonstrations are combined, it can be seen that the OH radicals have the most significant effect on bacteria inactivation. The OH radicals also damage cell membranes and lead to the degradation of DNA [24]. Its reaction with ozone and water by humidity produces OH radicals, which affect the rate of the reduction of airborne bacteria [29]. Figure 14 shows the reduction rate of airborne bacteria over the plasma treatment time through the 1 m^3 chamber sterilization module.

The experimental conditions are shown in Table 6. The experiment compares the results "without plasma" and "with plasma". In the "without plasma" case, this is the result of natural reduction. The natural reduction rate of bacteria shows a $33.6 \pm 4.8\%$ survival rate, a decrease of about 66.4% when neglected for 30 min. In the "with plasma" case,

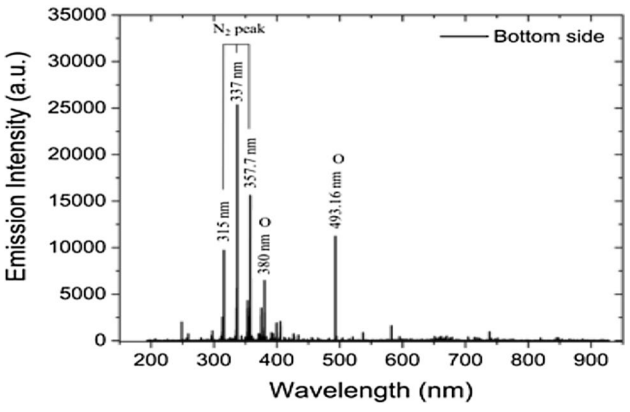

Fig. 13 Measured OES from 200 to 900 nm at a distance of 1 mm from the surface plasma with a power supply (integration time: 10 s, average: 10 times)

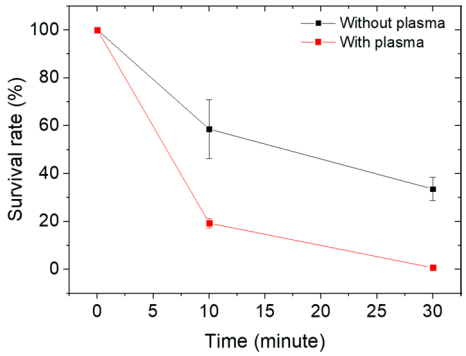

Fig. 14 Survival rate of *S. epidermidis* with plasma treatment for 30 min in a 1 m^3 chamber with 4 $kV_{pk\text{-}pk}$, 7.8 kHz

Table 6 Parameters and values of a sterilization experiment for airborne bacteria

Parameter	Value
Temperature	23.5 ± 2 ℃
Humidity	$50 \pm 5\%$
Initial condition	4×10^8 CFU/m^3

plasma treatment for 30 min, the survival rate of bacteria decreased by about 99.3%, which shows a survival rate of $0.7 \pm 0.5\%$. In previous studies, most of the plasma-based bacteria sterilization experiments were conducted by exposing plasma directly to a petri-dish where the bacteria were concentrated. Otherwise, a one pass duct system was used that passed through the DBD within a narrow space where the bacteria flowed [1, 3, 4, 28]. Although the rate of bacterial inactivation is much higher (log scales response) in the above systems, they are not suitable for indoor environments. Thus, this paper uses a circulating system for atmospheric air purification purposes. Therefore, the 99.3% airborne bacteria inactivation rate obtained from this study verifies that the purposed LLC inverter design can be effective for indoor air cleaning.

5 Conclusion

The performance of plasma ignition and sustainment is highly dependent on the power inverter system. In this paper, a half-bridge LLC inverter was adopted since it has advantages in terms of low cost and compact size for domestic plasma generators. A compact plasma generator design guide was established and applied to the SDBD structure. Here, the load (SDBD) was designed with a minimum capacitance of 10 pF to increase the output impedance and decrease the reactive power. In combination with the

designed driving circuit and the SDBD load, it provides a 7.8 kHz sinusoidal voltage of 4 $kV_{pk\text{-}pk}$. When the ROS and RNS are measured through a plasma generator by OES, the atomic oxygen spectrum and the second positive nitrogen system are enhanced. That means that various reactive species are produced. The 99.3% inactivation rate verifies that the proposed topology is suitable for driving the SDBD.

Acknowledgements This work was supported by the National Research Foundation of Korea (NRF) grant funded by the Korea government (MISP) (No. NRF-2019R1F1A1042084)

References

1. Kostov, K.G., Rocha, V., Koga-Ito, C.Y., Matos, B.M., Algatti, M.A., Honda, R.Y., Mota, R.P.: Bacterial sterilization by a dielectric barrier discharge (DBD) in air. Surf. Coat. Technol. **204**(18–19), 2954–2959 (2010)
2. Laroussi, M.: Sterilization of contaminated matter with an atmospheric pressure plasma. IEEE Trans. Plasma Sci. **24**(3), 1188–1191 (1996)
3. Lai, A.C.K., Cheung, A.C.T., Wong, M.M.L., Li, W.S.: Evaluation of cold plasma inactivation efficacy against different airborne bacteria in ventilation duct flow. Build. Environ. **98**, 39–46 (2016)
4. Helmke, A., Hoffmeister, D., Berge, F., Emmert, S., Laspe, P., Mertens, N., Vioel, W., Weltmann, K.D.: Physical and microbiological characterisation of *Staphylococcus epidermidis* inactivation by dielectric barrier discharge plasma. Plasma Process. Polym. **8**(4), 278–286 (2011)
5. Montie, T.C., Kelly-Wintenberg, K., Roth, J.R.: An overview of research using the one atmosphere uniform glow discharge plasma (OAUGDP) for sterilization of surfaces and materials. IEEE Trans. Plasma Sci. **28**(1), 41–50 (2000)
6. Eliasson, B., Hirth, M., Kogelschatz, U.: Ozone synthesis from oxygen in dielectric barrier discharges. J. Phys. D: Appl. Phys. **20**(11), 1421 (1987)
7. Wei, L.S., Yuan, D.K., Zhang, Y.F., Hu, Z.J., Dong, G.P.: Experimental and theoretical study of ozone generation in pulsed positive dielectric barrier discharge. Vacuum **104**, 61–64 (2014)
8. Chae, B., Min, J., Suh, Y., Kim, H., Kim, H.: Pulse current generator with improved waveform fidelity for high-voltage capacitively coupled plasma systems. J. Power Electron. **20**(5), 1316–1327 (2020)
9. Corke, T.C., Post, M.L., Orlov, D.M.: Single dielectric barrier discharge plasma enhanced aerodynamics: physics, modeling and applications. Exp. Fluids. **46**(1), 1–26 (2009)
10. Moshkunov, S.I., Podguyko, N.A., Shershunova, E.A.: Compact high voltage pulse generator for DBD plasma jets. J. Phys. Conf. Ser. **1115**(2), 022032 (2018)
11. Borghi, C.A., Cristofolini, A., Grandi, G., Neretti, G., Seri, P.: A plasma aerodynamic actuator supplied by a multilevel generator operating with different voltage waveforms. Plasma Sources Sci. Technol. **24**(4), 045018 (2015)
12. Florez, D., Schitz, D., Piquet, H., Diez, R.: Efficiency of an exciplex DBD lamp excited under different methods. IEEE Trans. Plasma Sci. **46**(1), 140–147 (2017)
13. Amjad, M., Salam, Z., Facta, M., Mekhilef, S.: Analysis and implementation of transformerless LCL resonant power supply for ozone generation. IEEE Trans. Power Electron. **28**(2), 650–660 (2012)
14. Lim, D., Uddin, N., Choi, S., Choi, D., Choi, J.: Dual microwave-excited atmospheric-pressure plasma jets with a single power source. Jpn. J. Appl. Phys. **60**(2), 026001 (2021)
15. Kwon, M. J., Lee, W. C.: A study on the analysis and control of no-load characteristics of LLC resonant converter for plasma process. In 2018 international power electronics conference. 114–117 (2018)
16. Pemen, A.J.M., Chirumamilla, V.R., Beckers, F.J.C.M., Hoeben, W.F.L.M., Huiskamp, T.: An SDBD plasma-catalytic system for on-demand air purification. IEEE Trans. Plasma Sci. **46**(12), 4078–4090 (2018)
17. Tudoran, C.D., Surducan, V., Simon, A., Papiu, A.M., Dinu, O.E., Anghel, S.D.: High frequency inverter based atmospheric pressure plasma treatment system. Rom. J. Phys. **57**, 1382–1391 (2012)
18. Pipa, A.V., Hink, R., Foest, R., Brandenburg, R.: Dependence of dissipated power on applied voltage for surface barrier discharge from simplest equivalent circuit. Plasma Sources Sci. Technol. **29**(12), 12LT01 (2020)
19. Bouanaka, F., Boudjadar, A., Rebiai, S.: Modeling and electrical characterization of atmospheric-pressure surface dielectric barrier discharge (SDBD) in Argon. In 2019 international conference on advanced electrical engineering (ICAEE). 1–6 (2019)
20. Kriegseis, J., Möller, B., Grundmann, S., Tropea, C.: Capacitance and power consumption quantification of dielectric barrier discharge (DBD) plasma actuators. J. Electrostat. **69**(4), 302–312 (2011)
21. Husain, E., Nema, R.S.: Analysis of Paschen curves for air, N2 and SF6 using the Townsend breakdown equation. IEEE Trans. Electr. Insul. **4**, 350–353 (1982)
22. Abdelaziz, A.A., Ishijima, T., Seto, T., Osawa, N., Wedaa, H., Otani, Y.: Characterization of surface dielectric barrier discharge influenced by intermediate frequency for ozone production. Plasma Sources Sci. Technol. **25**(3), 035012 (2016)
23. Choi, H.S., Choi, S.J.: Compact drive circuit for capacitive wireless power transfer system utilizing leakage-enhanced transformer. J. Electr. Eng. Technol. **14**(1), 191–199 (2019)
24. McLyman, C., William T.: Transformer and inductor design handbook. New York, USA (1988)
25. Kwon, M.J., Kim, T.H., Lee, W.C.: Analysis of the gain characteristic in LLCC resonant converter for plasma power supply. Trans. Korean Inst. Electr. Eng. **65**(12), 1992–1999 (2016)
26. Chen, Z., Amaro, I.: Optimizing low side gate resistance for damping phase node ringing of synchronous buck converter. In 2012 IEEE energy conversion congress and exposition (ECCE). 1827–1832 (2012)
27. Striney, J. A., Anuja, V., Ananth, M. B. J.: Design of integrated ZVS single-inductor synchronous buck converter for multiload applications. In 2016 international conference on electrical, electronics, and optimization techniques (ICEEOT). 4835–4840 (2016)
28. Dorai, R., Kushner, M.J.: A model for plasma modification of polypropylene using atmospheric pressure discharges. J. Phys. D: Appl. Physics. **36**(6), 666 (2003)
29. Choi, J.H., Han, I., Baik, H.K., Lee, M.H., Han, D.W., Park, J.C., Lee, I.S., Song, K.M., Lim, Y.S.: Analysis of sterilization effect by pulsed dielectric barrier discharge. J. Electrostat. **64**(1), 17–22 (2006)
30. Park, S., Park, J.Y., Choe, W.: Origin of hydroxyl radicals in a weakly ionized plasma-facing liquid. Chem. Eng. J. **378**, 122163 (2019)
31. Seo, D.C., Chung, T.H.: Observation of the transition of operating regions in a low-pressure inductively coupled oxygen plasma by langmuir probe measurement and optical emission spectroscopy. J. Phys. D: Appl Phys. **34**(18), 2854 (2001)

Yeong Woon Kim received his B.S. degree from the Department of Electronic and Electrical Engineering, University of Ulsan, Ulsan, Korea, in 2020. He is presently working towards his M.S. degree in School of Electronics and Electrical Engineering at Kyungpook National University, Daegu, Korea. He has been working as a Researcher at Korea Institue of Industrial Technology (KITECH), Ulsan, Korea. His current research interests include atmospheric pressure plasma and low-temperature plasma for environmental applications, and the design of an optimal power supply for plasma generation

Thusitha Wellawatta was born in Colombo, Sri Lanka. He received his B.S. degree in Electrical Engineering from the Engineering Council, London, ENG, UK, in 2012. From 2010 to 2014, he was with API Technologies, Colombo, Sri Lanka, where he worked as an Automation Engineer. Since 2014, he has been working as an Assistant Researcher in the School of Electrical Engineering, University of Ulsan, Ulsan, Korea, where he is also working towards his M.S. and Ph.D. degrees. Since 2020, he has been working as a Researcher at Korea Institute of Industrial Technology (KITECH), Ulsan, Korea. His current research interests include power electronics and control, including photovoltaic generation and utilization, maximum power tracking algorithms, PV partial shading algorithms, solar array simulators, and high voltage converters for plasma applications

Sung-Jin Choi received his B.S., M.S., and Ph.D. degrees in Electrical Engineering from Seoul National University, Seoul, Korea, in 1996, 1998, and 2006, respectively. From 2006 to 2008, he was working as a Research Engineer at Palabs Company, Ltd., Seoul, Korea. From 2008 to 2011, he was a Principal Research Engineer at Samsung Electronics Co., Ltd., Suwon, Korea, where he was responsible for developing LED drive circuits and wireless battery charging systems. In 2011, he joined the University of Ulsan, Ulsan, Korea, where he is presently working as an Professor in the School of Electrical Engineering. From 2017 to 2018, he was a Visiting Scholar at San Diego State University, San Diego, CA, USA. His current research interests include power processing technology related to solar power generation, battery management, and wireless power transfer

Jun Choi received his B.S. degree in Electronic and Electrical Engineering from Chung-Ang University, Seoul, Korea, in 2003, his M.S. and Ph.D. degrees in Electronic and Electrical Engineering from Pohang University of Science and Technology, Pohang, Korea, in 2005 and 2010, respectively. He is presently working as a Principal Researcher at Korea Institute of Industrial Technology (KITECH), Ulsan, Korea. His current research interests include low-temperature plasma, atmospheric-pressure glow discharge, and microwave-excited microplasma for industrial applications